

Electron correlations and T -breaking density wave order in a \mathbb{Z}_2 kagome metal

Chandan Setty^{⊕,†}, Haoyu Hu[⊕], Lei Chen, and Qimiao Si

Department of Physics & Astronomy, Rice Center for Quantum Materials, Rice University, Houston, Texas 77005, USA

There have been extensive recent developments on kagome metals, such as T_mX_n ($T = \text{Fe, Co}$ and $X = \text{Sn, Ge}$) and AV_3Sb_5 ($A = \text{Cs, K, Rb}$). An emerging issue is the nature of correlated phases when topologically *non-trivial* bands cross the Fermi level. Here, we consider an extended Hubbard model on the kagome lattice, involving a Kramers' pair of bands that have opposite Chern numbers and are isolated in the band structure. We construct an effective model in a time-reversal (T) symmetric lattice description. We determine the correlated phases of this model and identify a density-wave order in the phase diagram. We show that this order is T -breaking, which originates from the Wannier orbitals lacking a common Wannier center – a fingerprint of the underlying \mathbb{Z}_2 topology. Implications of our results for the correlation physics of the kagome metals are discussed.

Introduction: In standard settings of electron correlations, the effects of short-range repulsive Coulomb interactions are studied on topologically trivial Bloch bands. In the perturbative limit, interactions are exactly marginal and gapless excitations of the Fermi gas are retained in the Fermi liquid [1]. In contrast, correlated phases such as Mott insulators, charge density waves and nematic states typically emerge only when interactions become comparable to or greater than the overall non-interacting electron bandwidth (W_0) [2–4].

Correlated phases in systems such as twisted bilayer graphene [5, 6] on hexagonal boron nitride (TBG/hBN) [7], kagome lattice binary T_mX_n ($T = \text{Fe, Co}$ and $X = \text{Sn, Ge}$) [8–12] or ternary AV_3Sb_5 ($A = \text{Cs, K, Rb}$) [13–19] intermetallics and beyond [20] demand a fresh perspective to the aforementioned paradigm. These systems have a collection of topologically non-trivial bands [8, 21–26] close to the Fermi level. To isolate the effect of these bands, one may consider narrow bands (bandwidth W) [9, 10, 19, 27, 28] that are separated from the rest of the bands by a gap (Δ). Correlated phases would already emerge when (see Fig. 1(a))

$$U \sim W \ll \Delta < W_0, \quad (1)$$

indicating the necessity for low energy effective models obtained by projecting both the kinetic and interacting parts of the Hamiltonian on to only the narrow bands.

A key consequence of non-trivial topology for a given band is the well-known notion of topological obstruction [29–31] which is a double-edged sword. While it can substantially complicate the construction of reliable low-energy lattice models, it also presents an intriguing playground to isolate and examine the novel effects of topology [32–36] on well-known phases of matter previously obtained purely from trivial bands. These issues have yet to be considered for kagome metals [37–42], but are expected to be important to their understanding. They are also general issues that are broadly important to the physics of electron correlations as it intersects with that of electronic topology [2, 43].

In this Letter, we study the correlated phases of a kagome metal when its topologically nontrivial bands

cross the Fermi level. Importantly, we advance a non-perturbative framework that describes correlations in such topological metals (TMs), especially in the regime of Eq. 1. The applicability of a low energy effective lattice model in this regime with arbitrary partial fillings distinguishes this work from earlier attempts (see Ref. [44] for a review) to study interactions in topological models. First, Eq. 1 demands a non-perturbative treatment of correlations for experimentally relevant parameter values of U, W and Δ , which we offer here. Second, our treatment, applied in the context of partially filled Chern bands with arbitrary fillings, seeks to uncover hitherto unknown topological imprints on density wave orders. Finally, non-perturbative treatments of partially filled Chern bands that yield correlated metallic ground states (as we will see below) are exceedingly rare [44, 45]. These features of our work stand in stark contrast to earlier attempts at deriving fractional Chern insulating phases at very specific fillings [46–49], or mean-field orders which are unaffected by the topology of the underlying bands in the continuum limit (for a review, see Ref. [45]).

To this end, we examine an extended Hubbard model on the kagome lattice and isolate a Kramers' pair of bands with opposite Chern numbers crossing the Fermi level. Using Wannier orbitals suitable for topological bands whose nonzero Chern numbers add up to zero [31], we project the Coulomb interactions to these bands and construct an effective lattice model. We identify a T -breaking density wave (DW_t) metal in the phase diagram, and discuss its implications for the metallic kagome materials. Correlated metals of this sort have not been identified from partially filled topological bands in non-perturbative settings [44]. We further determine how the unusual nature of this phase is driven by the topological nature of the underlying bands and why it is absent in analogous phases derived from trivial bands. Our work highlights how the obstructive power of topology can be harnessed to drive novel correlated metallic phases.

Extended Hubbard model and topological obstruction:

The Hamiltonian is given by $\mathcal{H} = \mathcal{H}_0 + \mathcal{H}_I$ with

$$\begin{aligned} \mathcal{H}_0 = & -t \sum_{\langle ij \rangle \alpha \beta} c_{i\alpha}^\dagger c_{j\beta} + i\lambda_1 \sum_{\langle ij \rangle} (\mathbf{E}_{ij} \times \mathbf{R}_{ij}) \cdot c_{i\alpha}^\dagger \boldsymbol{\sigma} c_{j\beta} \\ & -t_2 \sum_{\langle\langle ij \rangle\rangle \alpha \beta} c_{i\alpha}^\dagger c_{j\beta} + i\lambda_2 \sum_{\langle\langle ij \rangle\rangle} (\mathbf{E}_{ij} \times \mathbf{R}_{ij}) \cdot c_{i\alpha}^\dagger \boldsymbol{\sigma} c_{j\beta} \\ \mathcal{H}_I = & \sum_{ij\alpha\beta} U_{j,\alpha\beta} n_{i\alpha} n_{i+j\beta} \quad . \end{aligned} \quad (2)$$

The kinetic part, \mathcal{H}_0 , describes electrons hopping on a kagome lattice in the presence of spin-orbit couplings (SOC) [46, 50]. Here $t(t_2)$ and $\lambda_1(\lambda_2)$ are the nearest neighbor (next-nearest neighbor) hopping and SOC respectively. \mathbf{R}_{ij} is the displacement vector from site i to site j and \mathbf{E}_{ij} is the electric field experienced along \mathbf{R}_{ij} . $c_{i\alpha}$ destroys an electron on site i and internal quantum number α , which refers to both sub-lattice and spin indices. The interaction part, \mathcal{H}_I , contains local interactions, including the on-site Hubbard interaction U and the nearest-neighbor (next-nearest neighbor) density-density interactions V (V'). They are expressed in terms of $U_{j,\alpha\beta}$ that couples the number operators $n_{i\alpha}$. We also denote the three triangular lattice vectors $\mathbf{n}_1 = 2a(\frac{1}{2}, \frac{\sqrt{3}}{2})$, $\mathbf{n}_2 = 2a(-\frac{1}{2}, \frac{\sqrt{3}}{2})$, $\mathbf{n}_3 = 2a(1, 0)$ where a is the nearest neighbor inter atomic spacing. For definiteness, we set $t_1 = 1, t_2 = -0.3, \lambda_1 = 0.28, \lambda_2 = 0.2$ [46]. These parameters give rise to the non-trivial topology in the band structure (see Fig. 1(a)) and splits the spectrum into three pairs of energetically well-separated degenerate bands with overall bandwidth $W_0 \sim 6$ and inter-band gaps of order $\Delta \sim 2.33$ (between the middle and bottom bands). Each pair at the top and bottom has Chern numbers ± 1 while the middle pair has zero Chern number each. The spinful \mathbb{Z}_2 TM is formed by partially filling the lowest pair of degenerate bands that have a small bandwidth $W \sim 0.04$. To study the correlation effect in the regime of Eq. 1, a reliable low energy effective lattice model with exponentially decaying projected interactions is essential. Topological obstruction complicates the construction of such a model as the projection hinges on the existence of exponentially localized Wannier functions. The latter are impossible when a Bloch discontinuity exists in the BZ that is incurable by a unitary gauge transformation of the band(s).

However, for a subspace of low-energy bands whose sum of Chern numbers vanishes, there exists a unitary transformation (U_T) that cures all discontinuities of the relevant Bloch functions while also respecting their reciprocal lattice vector periodicity [31, 51]. Our immediate goal, therefore, is to evaluate U_T that “smoothens” out the lowest pair of degenerate bands lying within an energy window W such that exponentially localized Wannier orbitals can be obtained while also preserving the Bravais periodicity. The procedure for evaluating U_T using the parallel transport gauge is briefly summarized in the Supplemental Material (SM) Sec. A.

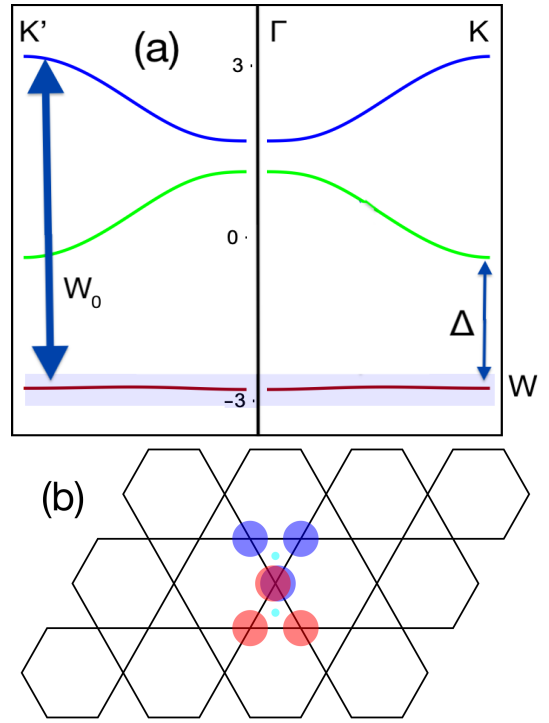


FIG. 1. (a) Plot of the non-interacting kagome bands with SOC. The effective model is projected on to the lowest pair of bands (blue rectangle) which have equal and opposite Chern numbers $C = \pm 1$. (b) Exponentially localized Wannier orbitals (WOs) (blue and red) that no longer share the same Wannier centers (cyan dots) due to non-trivial topology.

Wannier orbitals: We denote the final smoothed Bloch states (Figs. 4, 5, 7 of SM) as $|u_{f1}\rangle, |u_{f2}\rangle$, obtained from the initial states $|u_1\rangle, |u_2\rangle$ with Chern numbers ± 1 . The transformation that achieves this is $U_T \equiv U_H$, where U_H is defined as the matrix of eigenstates of the Haldane model also properly smoothed on a cylinder. In Fig. 3 of SM the geometric effect of applying U_H on the Wannier orbitals of $|u_1\rangle, |u_2\rangle$ is depicted. Before the action of U_H , the two Wannier orbitals share the same Wannier center, have equal onsite energies, and the corresponding Bloch states satisfy the Kramers' relations, $T|u_1\rangle_{\mathbf{k}} = |u_2\rangle_{-\mathbf{k}}$ and $T|u_2\rangle_{\mathbf{k}} = -|u_1\rangle_{-\mathbf{k}}$, where T is the time reversal operator. After the application of U_H , $|u_{f1}\rangle, |u_{f2}\rangle$ no longer satisfy the relations and hence do not form a Kramers' pair. The two corresponding Wannier orbitals have different Wannier centers, as shown in SM Fig. 3 (right panel) or Fig. 1(b), but are smooth in the momentum space and exponentially localized in the real space.

Denoting the operators for the Wannier orbitals in the new basis as $b_{\mathbf{k}\mu}$ ($\mu = 1, 2$), the following transformation properties under time-reversal hold

$$T\hat{\Psi}_{\mathbf{k}}T^{-1} = \hat{\mathcal{W}}(\mathbf{k})\hat{\Psi}_{-\mathbf{k}} \quad . \quad (3)$$

Here $\hat{\Psi}_{\mathbf{k}}$ is a column vector of the operators $b_{\mathbf{k}\mu}$ and $\hat{\mathcal{W}}(\mathbf{k})$ is a unitary matrix formed from sums of products

of U_H matrix elements (see SM Sec. A). Due to the aforementioned properties, the set of Bloch states $|u_{f1}\rangle, |u_{f2}\rangle$ now forms a convenient basis [52] to write an effective low-energy model with a minimal set of interaction and hopping parameters that respect translations. We also note that despite $|u_{f1}\rangle, |u_{f2}\rangle$ having zero Chern numbers, the topological imprints of the original \mathbb{Z}_2 TM are now encoded in the lack of a common Wannier center between the Wannier orbitals and revised definition of the time-reversal operator Eq. 3. Demanding time-reversal symmetry in the effective two-orbital Hamiltonian leads to additional non-local terms driven purely by the topology of the underlying bands and absent for trivial bands.

Projected lattice Hamiltonian: We are now equipped to project the local interactions U , V and V' of the original model, Eq. 2, onto the bands $|u_{f1}\rangle, |u_{f2}\rangle$. We denote $b_{i\mu}$ as the operator that destroys an electron at site i and Wannier orbital $\mu = 1, 2$ (WO 1, WO 2 for brevity). The total effective two orbital Hamiltonian (H) after projection is written as a sum of non-interacting band term (H_0) and interactions (H_I) given by

$$\begin{aligned} H &= H_0 + H_I \\ H_0 &= \sum_{ij} \sum_{\mu\nu} b_{i\mu}^\dagger t_{ij}^{\mu\nu} b_{j\nu} \\ H_I &= \sum_{ijkl} \sum_{m\nu\mu'\nu\nu'} u_{\mu\mu'\nu\nu'}(j, k, l) b_{i\mu}^\dagger b_{i+j\mu'} b_{i+k\nu}^\dagger b_{i+l\nu'} \end{aligned} \quad (4)$$

Here $t_{ij}^{\mu\nu}$ and $u_{\mu\mu'\nu\nu'}(j, k, l)$ are respectively the hopping parameters and interaction matrix elements, which are given in the SM (Tables I-III).

Several points are in order. First, in writing the interaction terms, transformation properties of the individual WOs under rotations and reflections must be considered in addition to the Bravais lattice symmetries. These properties are especially non-trivial since the two WOs no longer share the same Wannier center. All symmetries of the kagome lattice are respected once the transformation properties of individual WOs are taken into account. Second, although the two WOs now no longer form a Kramers' pair, the interaction Hamiltonian preserves time-reversal symmetry. The non-trivial effect of topology is now manifest in the non-local terms that follow from time-reversal invariance as well as the lack of a common center for the two WOs. With respect to the hopping parameters, the low-energy band structure can already be reproduced (see SM Fig. 6) from the effective model by truncating hopping parameters of the two WOs to the third neighbors.

Phase diagram and the nature of the DW_t order: We investigate the correlation effects via a $U(1)$ slave-spin method [53] (see SM, Sec. E). In the $U(1)$ slave spin method, we rewrite the electron operators as $b_{i\mu} = S_{i\mu}^- f_{i\mu}$ where f is the fermion operator and S^- is the spin operator. The original Hilbert space can be mapped onto an extended space of slave spins and f fermions according

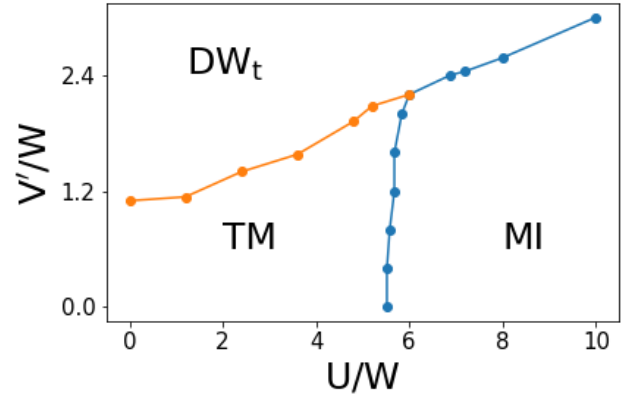


FIG. 2. Phase diagram of the model Hamiltonian in Eq. 4 expressed in terms of the interaction parameters of the original model, U and V' , in the unit of bandwidth W of the projected bands. The blue and orange lines denote first-order and second-order transitions respectively. The phase diagram involves topological metal (TM), T -breaking density wave order (DW_t), and Mott insulator (MI). In terms of the effective interactions of Eq. 4 (see Tables II and III, SM), the threshold values are ~ 0.35 (~ 0.14) along the horizontal (vertical) axis.

to the correspondence: $|1\rangle_b = |1\rangle_f |\uparrow\rangle_s$, $|0\rangle_b = |0\rangle_f |\downarrow\rangle_s$. To project out the unphysical degree of freedom, we enforce the constraint: $S_{i\mu}^z + \frac{1}{2} = f_{i\mu}^\dagger f_{i\mu}$. The slave spins carry the $U(1)$ charge which allows us to rewrite the four-WO interaction terms in Eq. 4 as $b_{i\mu}^\dagger b_{i\mu} b_{j\mu'} b_{j\mu'}^\dagger = (S_{i\mu}^z + \frac{1}{2})(S_{j\mu'}^z + \frac{1}{2})$. We then perform a Hubbard-Stratonovich decoupling of the spin terms above and solve the model at the saddle point level. The full Hamiltonian written in the slave-spin basis along with the self-consistent parameters is given in Sec. E of SM. We note that, due to the offset in the Wannier centers (*c.f.* Eq. 14, SM), the nearest neighbor interaction V plays a similar role as U in the effective model and, in particular, its tendency to drive a density wave order with an ordering wave vector K is reduced. Instead, V only modifies the phase boundaries, so we have set it to zero for convenience.

The phase diagram at half-filling is shown in Fig. 2. The horizontal and vertical axes are marked by the on-site and next-nearest neighbor interactions, U and V' respectively. The phase diagram contains three phases: a TM, Mott insulator (MI), and a density wave phase (DW_t), which has an ordering wave vector M . There are also three phase boundaries, and a tri-critical phase co-existence occurs around $(U/W, V'/W) \sim (6, 2.3)$. In the TM and DW_t phases, the quasi-particle weights remain nonzero and the system is metallic. In the MI phase, the quasi-particle weights vanish due to the interactions, and the electrons are localized. The Mott phase is also spontaneously T -breaking and characterized by a fully polarized ferro-orbital order in the WO basis which yields an in-plane spin order in the original kagome basis of Eq. 2.

We now turn to discussing the nature of the DW_t phase. This phase is a charge order when viewed in the

WO basis with a modulation vector at the M point. This is interesting since, in the absence of topology, a Kramers pair of WOs share the *same* Wannier center and a minimization of the onsite Coulomb repulsion would have instead yielded a (pure) spin order. In the current situation, due to the lack of a common center from the original topological bands, the *non-local* V' interaction instead drives a charge order at M point. Now when viewed in the original kagome basis, the DW_t contains a “collinear charge order” – a phase where the onsite charge density is modulated along the M direction; i.e., it acquires a gradient along one of the crystal axis direction but not the other – that is entwined with a collinear in-plane spin order by the \mathbb{Z}_2 topology. Due to the coexistence of the collinear charge and spin orders, the DW_t phase is naturally T-breaking. Such a property is absent in correlated phases derived from trivial bands. To see this, we write the charge operator and spin operator along x direction in the kagome basis as $\phi_{\mathbf{q}}^c = \sum_{\alpha} c_{\mathbf{k}\alpha}^{\dagger} c_{\mathbf{k}+\mathbf{q}\alpha}$ and $\phi_{\mathbf{q}}^x = \sum_{\alpha\gamma} \sigma_{\alpha\gamma}^x c_{\mathbf{k}\alpha}^{\dagger} c_{\mathbf{k}+\mathbf{q}\gamma}$ respectively. Switching to WO basis we obtain (see Sec. D of SM)

$$\begin{aligned}\phi_{\mathbf{q}}^c &\sim F(\mathbf{n}_1, \mathbf{n}_2) A^2 (n_{1,q} + n_{2,q}) + G(\mathbf{n}_1, \mathbf{n}_2) A^2 (n_{1,q} - n_{2,q}) \\ \phi_{\mathbf{q}}^x &\sim G(\mathbf{n}_1, \mathbf{n}_2) A^2 (n_{1,q} + n_{2,q}) + F(\mathbf{n}_1, \mathbf{n}_2) A^2 (n_{1,q} - n_{2,q})\end{aligned}$$

where $A \sim 0.5$ is the overlap constant, $n_{\mathbf{q}j}$ is the density operator for WO j and $F(\mathbf{n}_1, \mathbf{n}_2) = \frac{4+e^{iqn_1}+e^{-iqn_2}}{2}$, $G(\mathbf{n}_1, \mathbf{n}_2) = \frac{2-e^{iqn_1}-e^{-iqn_2}}{2}$. Consider the DW_t appearing in the phase diagram Fig. 2. This phase is a charge order in the WO basis with $n_{\mathbf{q}1} + n_{\mathbf{q}2} \sim \eta \delta_{\mathbf{q},M}$ and $n_{\mathbf{q}1} - n_{\mathbf{q}2} \sim 0$. Switching to the original kagome basis, it contributes to both charge and spin channels. A real space illustration of the intertwined nature of charge and spin degrees of freedom (defined with respect to the original kagome operators) is shown in Fig. 8 of SM. The \mathbf{n}_1 and $-\mathbf{n}_2$ vectors in the phase factors of Eq. 5 reflect the difference in the Wannier centers of the two WOs (see SM, Sec. C). Had they vanished, as for the WOs of topologically trivial bands, the mixing of the spin order into the charge order would have been absent, *despite* a non-zero SOC [54]. Hence this property is a direct consequence of the non-trivial \mathbb{Z}_2 topology of the kagome Hamiltonian.

Discussions: Several remarks are in order. First, the DW_t order is collinear and has an ordering wave vector M . At this level of energetics, all three M point orders in the BZ are feasible and hence degenerate. Further breaking of this degeneracy can occur once perturbations from coupling to the lattice via structural distortions is accounted for. In particular, such subleading energetics can lock the system into a $3Q$ order, which has the 2×2 real space pattern as observed in AV_3Sb_5 [13, 14]. We can additionally expect such an order to form a composite field that serves as an accompanying C_3 -breaking nematic order parameter, as has been found in recent experiments in KV_3Sb_5 [55] and studied in the context of

the moire systems [56]. We reserve a systematic study of the nematicity for a later work.

Second, we have considered a regime of parameters which facilitates a controlled theoretical analysis, with a particular form for SOC. Because the DW_t order appears as a phase, it is expected to be robust over an extended range of parameters and SOC types. Thus, even though in 3d-electron systems such as T_mX_n ($T = \text{Fe, Co}$ and $X = \text{Sn, Ge}$) and AV_3Sb_5 ($A = \text{Cs, K, Rb}$), the SOC is typically several percents of the overall bandwidth, we expect DW_t to be relevant. Finally, due to the involvement of Haldane eigenstates in the construction of the Hamiltonian Eq. 4, for ground states that feature non-trivial boundary physics one must treat the boundary physics by reverting to the original kagome basis.

Implications for Experiments: Several correlated phases [13–19] have been observed in AV_3Sb_5 . These systems have topological bands near their Fermi level, a key ingredient for the relevance of the DW_t phase. However, the width of these topological bands is intermediate and the strength of the correlations appears to be relatively weak, which suggests that the mixing of the spin order in the underlying charge density wave order will be relatively weak. These features are qualitatively consistent with the experimental observations. The charge order is indeed centered at the M point of the BZ [13–15, 18]. Both scanning tunneling microscopy (STM) [13] and anomalous Hall transport [57] measurements find evidence of chiral topological charge order that breaks time-reversal symmetry. In addition, μSR has so far found no evidence of static moments [58]. Thus, any spin order must be below the μSR resolution limit (see, however, “Note added” below). In the kagome lattice binary T_mX_n ($T = \text{Fe, Co}$ and $X = \text{Sn, Ge}$) compounds [8–11], flat bands are located about $\lesssim 0.3$ eV from the Fermi level [9, 21, 22], and the topological nature of the Fermi-level-crossing bands remains to be established. Because the correlation strength here is expected to be considerably larger than the 0.3 eV flat-band energy scale, we expect the latter to significantly influence the mechanism and nature of the correlated phases. Our work motivates the search for T-breaking charge-density-wave phases in the T_mX_n and related systems.

Conclusions: We studied correlation effects of a kagome metal when a pair of Z_2 topological bands with nonzero but opposite Chern numbers cross the Fermi level. Using a time-reversal symmetric lattice description, we constructed an effective lattice model and determined its correlated phase diagram. We identified a density-wave order that breaks time-reversal symmetry (DW_t) in the phase diagram. The phase originates from a Coulomb avoidance in a way that respects the topology of the underlying bands. We expect this mechanism to operate in broader contexts of correlated topological systems. The T-breaking density-wave order has important implications for understanding rapidly emerging ex-

periments in the ternary kagome metals. Such phases may also be explored by future experiments in the binary kagome systems as well as in other correlated metals whose crystalline lattice nurtures topological bands.

Acknowledgements: We thank P. C. Dai, Z. Guguchia and M. Yi for useful discussions. This work has in part been supported by the U.S. Department of Energy, Office of Science, Basic Energy Sciences, under Award No. DE-SC0018197 and the Robert A. Welch Foundation Grant No. C-1411 (Q.S.). Q.S. acknowledges the hospitality of the Aspen Center for Physics, which is supported by NSF grant No. PHY-1607611.

Note added: After this manuscript became available on the arXiv, two new μ SR [59, 60] and polar Kerr [61] measurements found evidence of broken time-reversal symmetry in the density wave phase of ternary Kagome systems. The μ SR data detect both in-plane and out-of-plane components of the broken time reversal symmetry supporting our findings.

⊕ These authors contributed equally to this work.

† csetty@rice.edu

-
- [1] R. Shankar, “Renormalization-group approach to interacting fermions,” *Reviews of Modern Physics* **66**, 129 (1994).
 - [2] Silke Paschen and Qimiao Si, “Quantum phases driven by strong correlations,” *Nature Reviews Physics* **3**, 9 (2021).
 - [3] Masatoshi Imada, Atsushi Fujimori, and Yoshinori Tokura, “Metal-insulator transitions,” *Rev. Mod. Phys.* **70**, 1039–1263 (1998).
 - [4] Antoine Georges, Gabriel Kotliar, Werner Krauth, and Marcelo J Rozenberg, “Dynamical mean-field theory of strongly correlated fermion systems and the limit of infinite dimensions,” *Reviews of Modern Physics* **68**, 13 (1996).
 - [5] Yuan Cao, Valla Fatemi, Ahmet Demir, Shiang Fang, Spencer L Tomarken, Jason Y Luo, Javier D Sanchez-Yamagishi, Kenji Watanabe, Takashi Taniguchi, Efthimos Kaxiras, *et al.*, “Correlated insulator behaviour at half-filling in magic-angle graphene superlattices,” *Nature* **556**, 80–84 (2018).
 - [6] Yuhang Jiang, Xinyuan Lai, Kenji Watanabe, Takashi Taniguchi, Kristjan Haule, Jinhai Mao, and Eva Y Andrei, “Charge order and broken rotational symmetry in magic-angle twisted bilayer graphene,” *Nature* **573**, 91–95 (2019).
 - [7] Aaron L Sharpe, Eli J Fox, Arthur W Barnard, Joe Finney, Kenji Watanabe, Takashi Taniguchi, MA Kastner, and David Goldhaber-Gordon, “Emergent ferromagnetism near three-quarters filling in twisted bilayer graphene,” *Science* **365**, 605–608 (2019).
 - [8] Linda Ye, Mingu Kang, Junwei Liu, Felix Von Cube, Christina R Wicker, Takehito Suzuki, Chris Jozwiak, Aaron Bostwick, Eli Rotenberg, David C Bell, *et al.*, “Massive dirac fermions in a ferromagnetic kagome metal,” *Nature* **555**, 638–642 (2018).
 - [9] Zhonghao Liu, Man Li, Qi Wang, Guangwei Wang, Chenhaoping Wen, Kun Jiang, Xiang Lu, Shichao Yan, Yaobo Huang, Dawei Shen, *et al.*, “Orbital-selective dirac fermions and extremely flat bands in frustrated kagome-lattice metal CoSn ,” *Nature communications* **11**, 1–7 (2020).
 - [10] Zhiyong Lin, Jin-Ho Choi, Qiang Zhang, Wei Qin, Seho Yi, Pengdong Wang, Lin Li, Yifan Wang, Hui Zhang, Zhe Sun, *et al.*, “Flatbands and emergent ferromagnetic ordering in Fe_3Sn_2 kagome lattices,” *Physical review letters* **121**, 096401 (2018).
 - [11] Enke Liu, Yan Sun, Nitesh Kumar, Lukas Muechler, Aili Sun, Lin Jiao, Shuo-Ying Yang, Defa Liu, Aiji Liang, Qian Xu, *et al.*, “Giant anomalous hall effect in a ferromagnetic kagome-lattice semimetal,” *Nature physics* **14**, 1125–1131 (2018).
 - [12] M Yao, H Lee, N Xu, Y Wang, J Ma, OV Yazyev, Y Xiong, M Shi, G Aeppli, and Y Soh, “Switchable Weyl nodes in topological Kagome ferromagnet Fe_3Sn_2 ,” arXiv:1810.01514 (2018).
 - [13] Yu-Xiao Jiang, Jia-Xin Yin, M Michael Denner, Nana Shumiya, Brenden R Ortiz, Junyi He, Xiaoxiong Liu, Songtian S Zhang, Guoqing Chang, Ilya Belopolski, *et al.*, “Unconventional chiral charge order in kagome superconductor Kv_3Sb_5 ,” *Nature Materials* **20**, 1353 (2021).
 - [14] He Zhao, Hong Li, Brenden R Ortiz, Samuel ML Teicher, Taka Park, Mengxing Ye, Ziqiang Wang, Leon Balents, Stephen D Wilson, and Ilija Zeljkovic, “Cascade of correlated electron states in a kagome superconductor CsV_3Sb_5 ,” *Nature* (2021), <https://doi.org/10.1038/s41586-021-03946-w>.
 - [15] Xiaoxiang Zhou, Yongkai Li, Xinwei Fan, Jiahao Hao, Yaomin Dai, Zhiwei Wang, Yugui Yao, and Hai-Hu Wen, “Origin of the Charge Density Wave in the Kagome Metal CsV_3Sb_5 as Revealed by Optical Spectroscopy,” arXiv e-prints, arXiv:2104.01015 (2021), arXiv:2104.01015 [cond-mat.supr-con].
 - [16] Zuwei Liang, Xingyuan Hou, Wanru Ma, Fan Zhang, Ping Wu, Zongyuan Zhang, Fanghang Yu, J-J Ying, Kun Jiang, Lei Shan, *et al.*, “Three-dimensional charge density wave and robust zero-bias conductance peak inside the superconducting vortex core of a kagome superconductor CsV_3Sb_5 ,” arXiv preprint arXiv:2103.04760 (2021).
 - [17] E Uykur, BR Ortiz, SD Wilson, M Dressel, and AA Tsirlin, “Optical detection of charge-density-wave instability in the non-magnetic kagome metal Kv_3Sb_5 ,” arXiv preprint arXiv:2103.07912 (2021).
 - [18] HX Li, TT Zhang, Y-Y Pai, C Marvinney, A Said, T Yilmaz, Q Yin, C Gong, Z Tu, E Vescovo, *et al.*, “Observation of unconventional charge density wave without acoustic phonon anomaly in kagome superconductors av_3sb_5 ($a = \text{rb, cs}$),” arXiv preprint arXiv:2103.09769 (2021).
 - [19] Yong Hu, Samuel ML Teicher, Brenden R Ortiz, Yang Luo, Shuting Peng, Linwei Huai, JZ Ma, NC Plumb, Stephen D Wilson, J-F He, *et al.*, “Charge-order-assisted topological surface states and flat bands in the kagome superconductor CsV_3Sb_5 ,” arXiv preprint arXiv:2104.12725 (2021).
 - [20] I. F. Gilmudinov, R. Schönemann, D. Vignolles, C. Proust, I. R. Mukhamedshin, L. Balicas, and H. Alloul, “Evidence for the coexistence between linearly dispersing bands and strong electronic correlations in the underlying kagome lattice of $\text{Na}_{2/3}\text{CoO}_2$,”

- arXiv:2101.05252 (2021).
- [21] Mingu Kang, Linda Ye, Shiang Fang, Jhih-Shih You, Abe Levitan, Minyong Han, Jorge I Facio, Chris Jozwiak, Aaron Bostwick, Eli Rotenberg, *et al.*, “Dirac fermions and flat bands in the ideal kagome metal fesn,” *Nature materials* **19**, 163–169 (2020).
 - [22] Mingu Kang, Shiang Fang, Linda Ye, Hoi Chun Po, Jonathan Denlinger, Chris Jozwiak, Aaron Bostwick, Eli Rotenberg, Efthimios Kaxiras, Joseph G Checkelsky, *et al.*, “Topological flat bands in frustrated kagome lattice cosn,” *Nature communications* **11**, 1–9 (2020).
 - [23] Zhi Li, Jincheng Zhuang, Li Wang, Haifeng Feng, Qian Gao, Xun Xu, Weichang Hao, Xiaolin Wang, Chao Zhang, Kehui Wu, *et al.*, “Realization of flat band with possible nontrivial topology in electronic kagome lattice,” *Science advances* **4**, eaau4511 (2018).
 - [24] Brenden R Ortiz, Samuel ML Teicher, Yong Hu, Julia L Zuo, Paul M Sarte, Emily C Schueller, AM Milinda Abeykoon, Matthew J Krogstad, Stephan Rosenkranz, Raymond Osborn, *et al.*, “Cs v 3 sb 5: A z 2 topological kagome metal with a superconducting ground state,” *Physical Review Letters* **125**, 247002 (2020).
 - [25] Brenden R Ortiz, Paul M Sarte, Eric M Kenney, Michael J Graf, Samuel ML Teicher, Ram Seshadri, and Stephen D Wilson, “Superconductivity in the z 2 kagome metal kv 3 sb 5,” *Physical Review Materials* **5**, 034801 (2021).
 - [26] Yang Fu, Ningning Zhao, Zheng Chen, Qiangwei Yin, Zhijun Tu, Chunsheng Gong, Chuanying Xi, Xiangde Zhu, Yuping Sun, Kai Liu, *et al.*, “Quantum transport evidence of topological band structures of kagome superconductor csv3sb5,” arXiv preprint arXiv:2104.08193 (2021).
 - [27] William R Meier, Mao-Hua Du, Satoshi Okamoto, Narayan Mohanta, Andrew F May, Michael A McGuire, Craig A Bridges, German D Samolyuk, and Brian C Sales, “Flat bands in the cosn-type compounds,” *Physical Review B* **102**, 075148 (2020).
 - [28] Zhiyong Lin, Chongze Wang, Pengdong Wang, Seho Yi, Lin Li, Qiang Zhang, Yifan Wang, Zhongyi Wang, Hao Huang, Yan Sun, *et al.*, “Dirac fermions in antiferromagnetic fesn kagome lattices with combined space inversion and time-reversal symmetry,” *Physical Review B* **102**, 155103 (2020).
 - [29] Christian Brouder, Gianluca Panati, Matteo Calandra, Christophe Mourougane, and Nicola Marzari, “Exponential localization of wannier functions in insulators,” *Physical review letters* **98**, 046402 (2007).
 - [30] Nicola Marzari, Arash A Mostofi, Jonathan R Yates, Ivo Souza, and David Vanderbilt, “Maximally localized wannier functions: Theory and applications,” *Reviews of Modern Physics* **84**, 1419 (2012).
 - [31] Alexey A Soluyanov and David Vanderbilt, “Smooth gauge for topological insulators,” *Physical Review B* **85**, 115415 (2012).
 - [32] Hoi Chun Po, Liujun Zou, Ashvin Vishwanath, and T Senthil, “Origin of mott insulating behavior and superconductivity in twisted bilayer graphene,” *Physical Review X* **8**, 031089 (2018).
 - [33] Ya-Hui Zhang, Dan Mao, Yuan Cao, Pablo Jarillo-Herrero, and T Senthil, “Nearly flat chern bands in moiré superlattices,” *Physical Review B* **99**, 075127 (2019).
 - [34] Ya-Hui Zhang and T Senthil, “Bridging hubbard model physics and quantum hall physics in trilayer graphene/h-bn moiré superlattice,” *Physical Review B* **99**, 205150 (2019).
 - [35] Nishchhal Verma, Tamaghna Hazra, and Mohit Randeria, “Optical spectral weight, phase stiffness and tc bounds for trivial and topological flat band superconductors,” arXiv preprint arXiv:2103.08540 (2021).
 - [36] Jie Wang, Jennifer Cano, Andrew J Millis, Zhao Liu, and Bo Yang, “Exact landau level description of geometry and interaction in a flatband,” arXiv preprint arXiv:2105.07491 (2021).
 - [37] Andreas Mielke, “Ferromagnetic ground states for the hubbard model on line graphs,” *Journal of Physics A: Mathematical and General* **24**, L73 (1991).
 - [38] A Mielke, “Exact ground states for the hubbard model on the kagome lattice,” *Journal of Physics A: Mathematical and General* **25**, 4335 (1992).
 - [39] Jun Wen, Andreas Rüegg, C.-C. Joseph Wang, and Gregory A. Fiete, “Interaction-driven topological insulators on the kagome and the decorated honeycomb lattices,” *Phys. Rev. B* **82**, 075125 (2010).
 - [40] Xilin Feng, Kun Jiang, Ziqiang Wang, and Jiangping Hu, “Chiral flux phase in the kagome superconductor av3sb5,” *Science Bulletin* (2021).
 - [41] M Michael Denner, Ronny Thomale, and Titus Neupert, “Analysis of charge order in the kagome metal a v $_{3sb}$ $_{5}(a = k, rb, cs)$,” arXiv preprint arXiv:2103.14045 (2021).
 - [42] Yu-Ping Lin and Rahul M Nandkishore, “Complex charge density waves at van hove singularity on hexagonal lattices: Haldane-model phase diagram and potential realization in kagome metals a v $_{3sb}$ $_{5}$,” arXiv preprint arXiv:2104.02725 (2021).
 - [43] Robert Schaffer, Eric Kin-Ho Lee, Bohm-Jung Yang, and Yong Baek Kim, “Recent progress on correlated electron systems with strong spin-orbit coupling,” *Rep. Prog. Phys.* **79**, 094504 (2016).
 - [44] Stephan Rachel, “Interacting topological insulators: a review,” *Reports on Progress in Physics* **81**, 116501 (2018).
 - [45] Michael M Fogler, “Stripe and bubble phases in quantum hall systems,” in *High Magnetic Fields* (Springer, 2002) pp. 98–138.
 - [46] Evelyn Tang, Jia-Wei Mei, and Xiao-Gang Wen, “High-temperature fractional quantum hall states,” *Physical review letters* **106**, 236802 (2011).
 - [47] Titus Neupert, Luiz Santos, Claudio Chamon, and Christopher Mudry, “Fractional quantum hall states at zero magnetic field,” *Physical review letters* **106**, 236804 (2011).
 - [48] Kai Sun, Zhengcheng Gu, Hosho Katsura, and S Das Sarma, “Nearly flatbands with nontrivial topology,” *Physical review letters* **106**, 236803 (2011).
 - [49] Nicolas Regnault and B Andrei Bernevig, “Fractional chern insulator,” *Physical Review X* **1**, 021014 (2011).
 - [50] H.-M. Guo and M. Franz, “Topological insulator on the kagome lattice,” *Phys. Rev. B* **80**, 113102 (2009).
 - [51] Alexey A Soluyanov and David Vanderbilt, “Wannier representation of z 2 topological insulators,” *Physical Review B* **83**, 035108 (2011).
 - [52] It is worth emphasizing that, since U_H is a unitary gauge transformation that is smooth only on a cylinder due to the non-trivial topology of the Haldane model, observables of two Hamiltonians formed by the two sets of Wannier orbitals are only invariant in the absence of a boundary. Hence the predictions of the two models –

- provided one is able to construct a low energy Hamiltonian from $|u_1\rangle, |u_2\rangle$ – are the same as long as only bulk properties are probed ().
- [53] Rong Yu and Qimiao Si, “ $u(1)$ slave-spin theory and its application to mott transition in a multiorbital model for iron pnictides,” *Phys. Rev. B* **86**, 085104 (2012).
 - [54] Since the order parameter for our charge order is a scalar, it does not couple to spin degrees through SOC. This is unlike other vectorial density-wave order parameters studied in the context of loop current orders. ().
 - [55] Hong Li, He Zhao, Brenden R Ortiz, Takamori Park, Mengxing Ye, Leon Balents, Ziqiang Wang, Stephen D Wilson, and Ilija Zeljkovic, “Rotation symmetry breaking in the normal state of a kagome superconductor kv3sb5,” *arXiv preprint arXiv:2104.08209* (2021).
 - [56] Lei Chen, Haoyu Hu, and Qimiao Si, “Fragile insulator and electronic nematicity in a graphene moiré system,” *arXiv preprint arXiv:2007.06086* (2020).
 - [57] Shuo-Ying Yang, Yaojia Wang, Brenden R Ortiz, Defa Liu, Jacob Gayles, Elena Derunova, Rafael Gonzalez-Hernandez, Libor Šmejkal, Yulin Chen, Stuart SP Parkin, *et al.*, “Giant, unconventional anomalous hall effect in the metallic frustrated magnet candidate, kv3sb5,” *Science advances* **6**, eabb6003 (2020).
 - [58] Eric M Kenney, Brenden R Ortiz, Chennan Wang, Stephen D Wilson, and Michael Graf, “Absence of local moments in the kagome metal kv3sb5 as determined by muon spin spectroscopy,” *Journal of Physics: Condensed Matter* (2021).
 - [59] C. Mielke III au2, D. Das, J. X. Yin, H. Liu, R. Gupta, C. N. Wang, Y. X. Jiang, M. Medarde, X. Wu, H. C. Lei, J. J. Chang, P. Dai, Q. Si, H. Miao, R. Thomale, T. Neupert, Y. Shi, R. Khasanov, M. Z. Hasan, H. Luetkens, and Z. Guguchia, “Time-reversal symmetry-breaking charge order in a correlated kagome superconductor,” (2021), *arXiv:2106.13443 [cond-mat.mtrl-sci]*.
 - [60] Li Yu, Chennan Wang, Yuhang Zhang, Mathias Sander, Shunli Ni, Zouyouwei Lu, Sheng Ma, Zhengguo Wang, Zhen Zhao, Hui Chen, Kun Jiang, Yan Zhang, Haitao Yang, Fang Zhou, Xiaoli Dong, Steven L. Johnson, Michael J. Graf, Jiangping Hu, Hong-Jun Gao, and Zhongxian Zhao, “Evidence of a hidden flux phase in the topological kagome metal csv3sb5,” (2021), *arXiv:2107.10714 [cond-mat.supr-con]*.
 - [61] Qiong Wu, Z. X. Wang, Q. M. Liu, R. S. Li, S. X. Xu, Q. W. Yin, C. S. Gong, Z. J. Tu, H. C. Lei, T. Dong, and N. L. Wang, “The large static and pump-probe kerr effect with two-fold rotation symmetry in kagome metal csv3sb5,” (2021), *arXiv:2110.11306 [cond-mat.supr-con]*.

SUPPLEMENTAL MATERIAL

A. Parallel transport

Topological obstruction is the lack of a smooth Bloch representation for a given band throughout the Brillouin zone (BZ) which also respects symmetries of the Bravais lattice. Such obstruction, depending on the type, can substantially complicate the construction of reliable low-energy lattice models that are necessary to treat the correlated system's need to avoid the Coulomb repulsion. In situations which the obstruction can be resolved, like the specific case we discuss in this work, a key task is to determine the unitary band transformation matrix U_T for each \mathbf{k} point in the Brillouin zone grid that untangles the topology. Below we outline the steps for evaluating the form of U_T and applying it to the Bloch states in our problem.

Determining the form of U_T for specific systems can be a non-trivial task that depends on the lattice structure and the degree of Wannier localization desired. The simplest procedure [51] involves projecting the n Bloch states onto an *ansatz* of n trial states and using the determinant of the resulting $n \times n$ matrix to renormalize the original Bloch functions. This procedure was used to derive reliable tight-binding description in moire superlattices [32–34] and recently implemented in Lieb lattices [35] to derive bounds on superfluid stiffness. An obvious difficulty with the projection method, however, is the requirement of a suitable *ansatz* with the correct symmetries. The initial guess becomes harder with more quantum numbers, increased size of Hilbert space and complex lattice geometry. In the case of the kagome lattice, even if the correct symmetry of the wave functions is used as a guess, non-singular wave function normalization throughout the BZ is not assured. To circumvent this difficulty, we instead use the more intuitive parallel transport gauge [31] from which U_T can be obtained more readily.

In this section, we briefly outline the various steps involved in obtaining the parallel transport gauge used for the kagome problem and refer the reader to Ref. [31] for further details. First, through a linear transformation, the two low-lying Bloch functions, $|u_1\rangle, |u_2\rangle$, with Chern numbers ± 1 and bandwidth W are redefined on a rectangular BZ where $\tilde{k}_x \in [0, 2\pi]$, $\tilde{k}_y \in [-\pi, \pi]$. Next, the states are parallel transported along $\tilde{k}_y = 0$ and the continuity between $\tilde{k}_x = 0$ and $\tilde{k}_x = 2\pi$ is restored by redistributing the total phase along the $\tilde{k}_y = 0$ line. In the third step, for every \tilde{k}_x , two directionally opposite parallel transports are carried out – one from $(\tilde{k}_x, 0)$ to (\tilde{k}_x, π) , and another from $(\tilde{k}_x, 0)$ to $(\tilde{k}_x, -\pi)$. In the next step, periodicity along \tilde{k}_y is restored at $\tilde{k}_x = 0$ and $\tilde{k}_x = 2\pi$ while an off-diagonal unitary matrix, $V(\tilde{k}_x)$, connects the two states for every remaining \tilde{k}_x . In the penultimate step, the two Bloch states are untangled by diagonalizing the matrix $V(\tilde{k}_x)$ without disturbing their smoothness in rest of the BZ. At this stage, one is left with a Kramers' pair of bands with Chern numbers ± 1 that is periodic with respect to reciprocal vectors along \tilde{k}_x but not along \tilde{k}_y for each \tilde{k}_x except $\tilde{k}_x = 0, 2\pi$, i.e., they are smooth on a cylinder. In the final step, the Bloch states are rotated into a gauge that is smooth on a torus by using the eigenstates of the Haldane model (U_H) that have Chern numbers ± 1 . The Haldane matrix U_H , properly smoothened on a cylinder, plays the role of U_T and rotates the original Bloch states into a trivial basis $|u_{f1}\rangle, |u_{f2}\rangle$ with zero Chern numbers each. The topological obstruction is thus resolved. Certain real and imaginary components of $|u_{f1}\rangle$ and $|u_{f2}\rangle$ are plotted in Fig. 4 and the exponential decay of the Wannier functions is shown in Fig. 5.

The linear transformation matrix U_T is defined as the matrix (U_H) of eigenvectors of the Haldane model

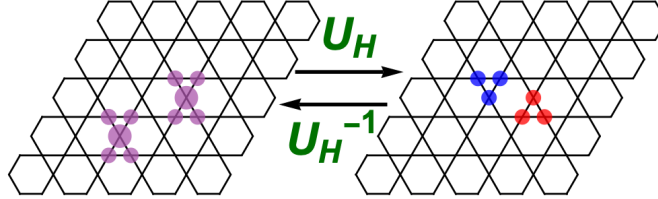


FIG. 3. Wannier orbitals before (left) and after (right) Haldane rotation. On the left panel, the Wannier orbitals share a common Wannier center and form a Kramers' pair. On the right panel, the Wannier orbitals lack a common Wannier center and break Kramers' relations, but their Bloch states instead satisfy the more general Eq. 3.

properly smoothened on a cylinder according to the prescription detailed above. We denote these matrix elements as

$g_{ij}(\mathbf{k})$. Using this matrix for U_T

$$U_T \equiv U_H = \begin{bmatrix} g_{11}(\mathbf{k}) & g_{12}(\mathbf{k}) \\ g_{21}(\mathbf{k}) & g_{22}(\mathbf{k}) \end{bmatrix}, \quad (5)$$

the unitary matrix $\hat{\mathcal{U}}(\mathbf{k})$ which defines the action of time reversal operator T on the operators $d_{\mathbf{k}\mu}$ in the main text is given by

$$\hat{\mathcal{U}}(\mathbf{k}) = \begin{bmatrix} (g_{11}^*(\mathbf{k})g_{21}(-\mathbf{k}) + g_{12}^*(\mathbf{k})g_{22}(-\mathbf{k})) & (-g_{11}^*(\mathbf{k})g_{11}(-\mathbf{k}) - g_{12}^*(\mathbf{k})g_{12}(-\mathbf{k})) \\ (g_{21}^*(\mathbf{k})g_{21}(-\mathbf{k}) + g_{22}^*(\mathbf{k})g_{22}(-\mathbf{k})) & (-g_{21}^*(\mathbf{k})g_{11}(-\mathbf{k}) - g_{22}^*(\mathbf{k})g_{12}(-\mathbf{k})) \end{bmatrix}. \quad (6)$$

B. Projected Hamiltonian in the Wannier basis

In this section, we derive the effective model in the WO basis. We start from the extended Hubbard model with Coulomb interactions on the kagome lattice.

$$\mathcal{H} = \mathcal{H}_0 + \mathcal{H}_I$$

$$\mathcal{H}_0 = \sum_{ij\alpha\beta} c_{i\alpha}^\dagger T_{ij,\alpha\beta} c_{j\beta} \quad (7)$$

$$\mathcal{H}_I = \sum_{ij\alpha\beta} U_{j,\alpha\beta} n_{i\alpha} n_{i+j\beta} \quad (8)$$

The hopping matrix can be diagonalized by V_k^\dagger with $V_k T_k V_k^\dagger = \text{diag}(\epsilon_{k,1}, \epsilon_{k,2}, \dots)$. We then introduce the band basis $d_{\mathbf{k}} = V_{\mathbf{k}} c_{\mathbf{k}}$ and projection operator $P = \prod_{\mathbf{k}, \mu > 2} (1 - d_{\mathbf{k}\mu}^\dagger d_{\mathbf{k}\mu})$. It's not difficult to show $P d_{\mathbf{k}\mu} P = d_{\mathbf{k}\mu}$ for $\mu = 1, 2$ and

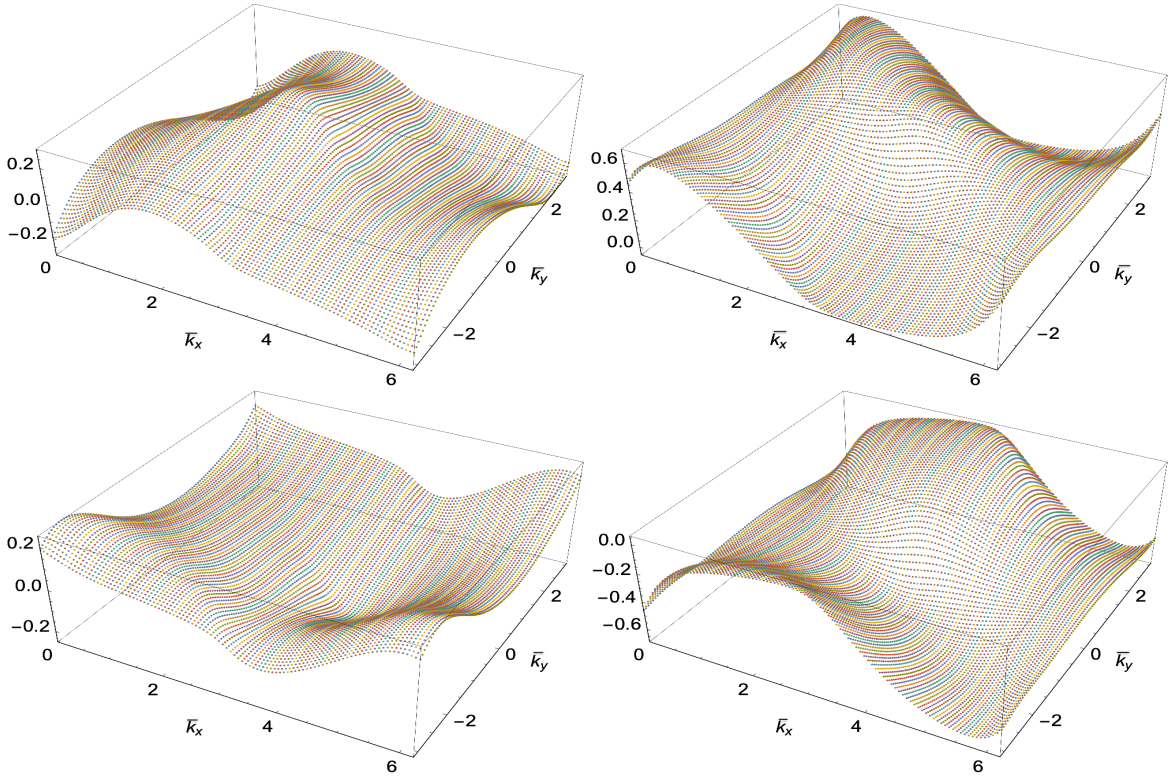


FIG. 4. Example plots of Bloch functions in the rescaled and rotated rectangular Brillouin zone after the Wannierization process. (Top row) Real (left) and imaginary (right) parts of fourth component of $|u_{f1}\rangle$. (Bottom row) Same as top row but for $|u_{f2}\rangle$.

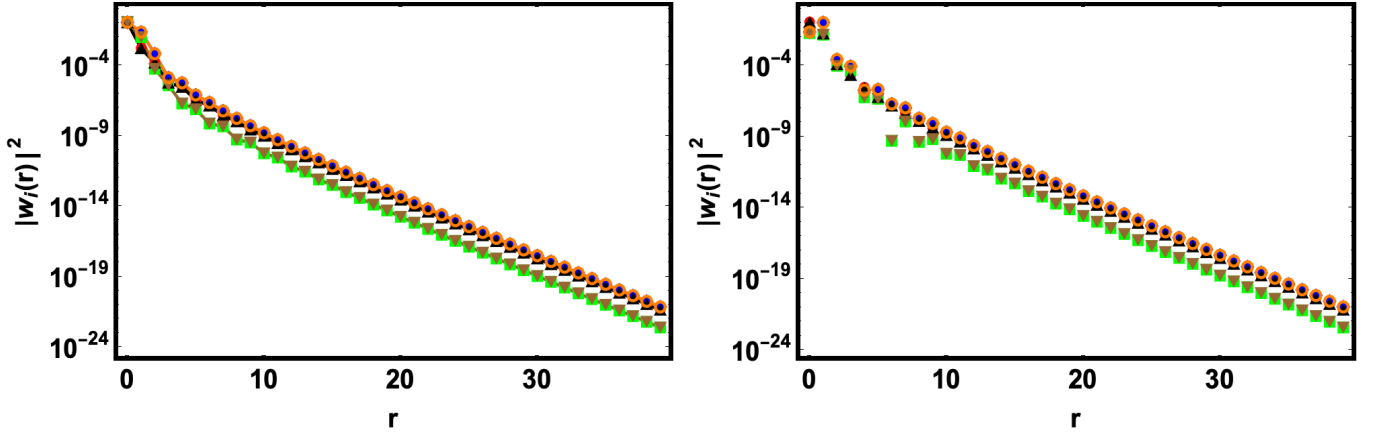


FIG. 5. Plots of probability density along the six projections of the first (left) and second (right) Bloch states as a function of distance from Wannier center.

$Pd_{\mathbf{k}\mu}P = 0$ for $\mu > 2$. The projection operator would only keep the lowest two bands and project out the high energy degrees of freedom. The effective Hamiltonian is defined as

$$H = P\mathcal{H}P \quad (9)$$

Since the lowest two bands have non-trivial topology, the Hamiltonian in the band basis contains long-range interactions. In order to derive a local Hamiltonian with exponentially decayed interactions, we introduce the WOs as described in previous section $b_{\mathbf{k}} = U_{H,\mathbf{k}}d_{\mathbf{k}}$. In the WO basis, it's not difficult to show:

$$Pc_{\mathbf{k}\mu}P = \sum_{\mu} (V_{\mathbf{k}}^{\dagger}U_{H,\mathbf{k}}^{\dagger})_{\mu\nu}b_{\mathbf{k}\nu} \quad (10)$$

Then we can replace all the terms in the Hamiltonian with their projected formula and then the effective Hamiltonian reads

$$\begin{aligned} H &= H_0 + H_I \\ H_0 &= \sum_{\substack{i,j \\ \mu,\nu}} b_{i\mu}^{\dagger} t_{ij}^{\mu\nu} b_{j\nu} \\ H_I &= \sum_{\substack{i,j,k,l \\ \mu,\mu',\nu,\nu'}} u_{\mu\mu'\nu\nu'}(j,k,l) b_{i\mu}^{\dagger} b_{i+j\mu'} b_{i+k\nu}^{\dagger} b_{i+l\nu'} \end{aligned} \quad (11)$$

where

$$\begin{aligned} t_{ij}^{\mu\nu} &= \sum_{\mu'\nu'i'j'} T_{i'j'}^{\mu'\nu'} w_{\mu',i'-i}^* w_{\nu',j'-j} \\ u_{\mu\nu\mu'\nu'}(j,k,l) &= \sum_{e,i,\alpha\gamma} U_{e,\alpha\gamma} w_{\alpha\mu,i}^* w_{\alpha\nu,i-j} w_{\gamma\mu',i-k+e}^* w_{\gamma\nu',i-l+e} \quad , \end{aligned} \quad (12)$$

and $w_{\alpha\nu,i} = \frac{1}{N} \sum_{\mathbf{k}} (V_{\mathbf{k}}^{\dagger}U_{H,\mathbf{k}}^{\dagger})_{\mu\nu} e^{i\mathbf{k}\cdot\mathbf{r}_i}$ denotes the real space wave functions of WOs.

The hopping parameters of the original kagome lattice are: $t_1 = 1, t_2 = -0.3, \lambda_1 = 0.28, \lambda_2 = 0.2$. The effective hopping takes form of $t_{ij}^{\mu\nu} = \delta_{\mu\nu} t_{j-i}$. We truncate to the third-neighbor hopping and list the hopping strength in Table I. In Fig. 6, we compare the original band structures with the dispersion generated by Table I and a good consistency is seen.

For the interaction term, we consider the onsite-Hubbard interactions U , the nearest-neighbor Coulomb interactions V and next-nearest-neighbor Coulomb interactions V' in the original kagome models. These would generate various interaction terms in the effective model. The numerical values of each term are shown in Table II and Table III. For the terms generated by U , we omit ones that are less than 10% of the leading-order contributions. For the terms generated by V, V' , we only keep the leading order contributions, The sub-leading part is about 30% of the leading-order contributions. Even though various types of interactions could be induced, all the terms in the Hamiltonian are exponentially decayed.

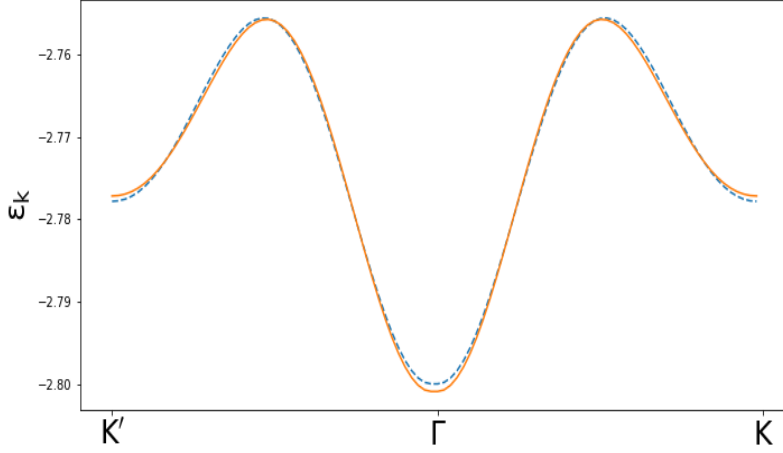


FIG. 6. A comparison of dispersions along high symmetry lines of the lowest degenerate doublet of kagome bands. Dashed line is the original kagome band and solid line is from the effective model with Wannier orbitals.

n, m	(0,1)	(1,0)	(0,-1)	(-1,0)	(-1,-1)	(1,1)
$t_{n\mathbf{n}_1+m\mathbf{n}_2}$	-0.000698	-0.000698	-0.000698	-0.000698	-0.000698	-0.000698
n, m	(-2,0)	(2,0)	(0,2)	(0,-2)	(-2,-2)	(2,2)
$t_{n\mathbf{n}_1+m\mathbf{n}_2}$	-0.001945	-0.001945	-0.001945	-0.001945	-0.001945	-0.001945
n, m	(-2,-1)	(-1,-2)	(-1,1)	(1,-1)	(1,2)	(2,1)
$t_{n\mathbf{n}_1+m\mathbf{n}_2}$	-0.003026	-0.003026	-0.003026	-0.003026	-0.003026	-0.003026

TABLE I. Hopping parameters in the WO basis

C. Real space Wannier functions and approximate Hamiltonian

We now turn to the real-space pattern of WOs and the approximate Hamiltonian. After constructing the WOs from the smooth gauge, we also use the standard maximal-localization procedure to make the Wannier orbitals even more localized. The final amplitude of two WOs are shown in Fig. 7

Approximately, the leading contributions of each WO come from three sites (marked as blue points in Fig. 7). It

m, n	μ, ν	$u_{\mu\mu\nu}(0, m\mathbf{n}_1 + n\mathbf{n}_2, m\mathbf{n}_1 + n\mathbf{n}_2)$
0,0	0,1	$0.078U + 0.320V + 0.146V'$
-1,0	0,1	$0.078U + 0.320V + 0.146V'$
0,1	0,1	$0.078U + 0.320V + 0.146V'$
-1,-1	0,1	$0.033V + 0.142V'$
1,1	0,1	$0.033V + 0.142V'$
-1,1	0,1	$0.033V + 0.142V'$
1,0	0,0	$0.066V + 0.142V'$
0,1	0,0	$0.066V + 0.142V'$
1,1	0,0	$0.066V + 0.142V'$
1,0	1,1	$0.066V + 0.142V'$
0,1	1,1	$0.066V + 0.142V'$
1,1	1,1	$0.066V + 0.142V'$

TABLE II. Interaction terms in the WO basis (part I).

m, n, k, l	μ, ν	$u_{\mu\nu\nu}(0, 0, m\mathbf{a}_1 + n\mathbf{n}_2, k\mathbf{a}_1 + l\mathbf{n}_2)$	m, n, k, l	μ, ν	$u_{\mu\nu\nu}(0, 0, m\mathbf{a}_1 + n\mathbf{n}_2, k\mathbf{a}_1 + l\mathbf{n}_2)$
0,1,0,0	0,1	0.02U	1,0,0,0	0,1	0.016U
0,0,0,-1	1,0	0.02U	0,0,-1,0	1,0	0.016U
0,-1,0,0	1,0	0.02U	-1,0,0,0	1,0	0.016U
0,0,0,1	1,0	0.02U	0,0,1,0	1,0	0.016U
0,0,0,1	0,1	0.02U	0,0,1,0	0,1	0.016U
0,1,0,0	0,1	0.02U	1,0,0,0	0,1	0.016U
0,0,0,1	0,1	0.02U	0,0,1,0	0,1	0.016U
0,-1,0,0	1,0	0.02U	-1,0,0,0	1,0	0.016U
1,0,0,1	1,0	0.018U	0,1,1,0	0,1	0.018U
-1,1,0	1,0	0.018U	-1,0,0,1	0,1	0.018U
1,0,0,-1	1,0	0.018U	0,1,-1,0	0,1	0.018U
0,-1,1,0	1,0	0.018U	-1,0,0,1	0,1	0.018U

TABLE III. Interaction terms in the WO basis (part II).

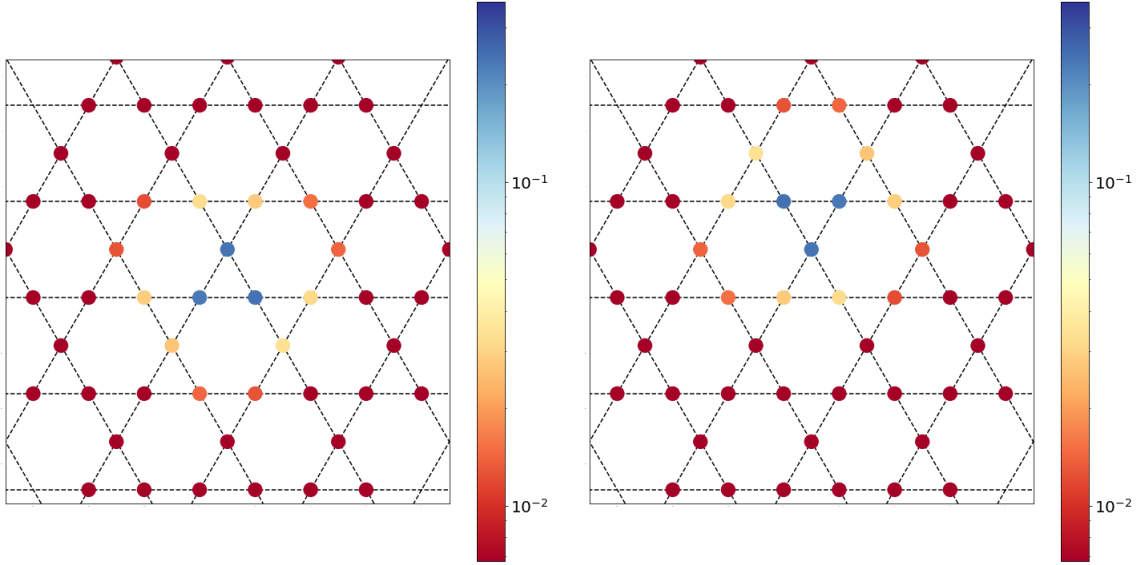


FIG. 7. Probability distributions of two maximally localized WOs.

allows us to construct the approximate formula of WOs

$$\begin{aligned}
b_{r,1}^\dagger &\sim A(c_{r,a+}^\dagger + c_{r,b+}^\dagger + c_{r,c+}^\dagger) \\
b_{r,2}^\dagger &\sim A(c_{r+\mathbf{n}_1,a-}^\dagger + c_{r-\mathbf{n}_2,b-}^\dagger + c_{r,c-}^\dagger)
\end{aligned} \tag{13}$$

Here we are using the eigenstates of S^x : $|\pm\rangle = \frac{1}{\sqrt{2}}|\uparrow \pm \downarrow\rangle$. a, b, c denotes three sub-lattices located at $(-1/4, \sqrt{3}/4), (1/4, \sqrt{3}/4), (0, \sqrt{3}/2)$. Numerically, we find $A \sim 0.5$ and the sub-leading contributions from each site is less than 10%.

We want to emphasize that the two WOs don't have a common center in the topological non-trivial case (even after the maximal-localization procedure). The sum of two Wannier centers \bar{r} is a gauge-invariant quantity and won't change during the localization procedure. It lies at the center of the hexagon (setting one center of the hexagon as the origin) in the topological non-trivial case. If we maximally localized one of the Wannier orbitals, its Wannier center lies at the center of the triangular. Consequently, the center of another Wannier orbitals has to deviate from the first one in order to make \bar{r} stay at the center of the hexagon. However, in a topological trivial case, we can always make two WOs be Kramers doublets; in turn, the two WOs have a common center due to the time-reversal symmetry.

According to the approximate formula in Eq. 13, we can also write the approximate interactions as:

$$\begin{aligned}
H_I = & \sum_{ij} (U + 4V + 4V') A^4 b_{1i}^\dagger b_{1i} (\delta_{j,i} + \delta_{j,i-\mathbf{n}_1} + \delta_{j,i+\mathbf{n}_2}) b_{2j}^\dagger b_{2j} \\
& + \sum_{ij,\mu} (V + 2V') A^4 b_{\mu i}^\dagger b_{\mu i} (\delta_{j,i+\mathbf{n}_1} + \delta_{j,i+\mathbf{n}_2} + \delta_{j,i+\mathbf{n}_1+\mathbf{n}_2}) b_{\mu j}^\dagger b_{\mu j} \\
& + \sum_{ij,\mu} 2V' A^4 b_{1i}^\dagger b_{1i} (\delta_{j,i+\mathbf{n}_1+\mathbf{n}_2} + \delta_{j,i-\mathbf{n}_1-\mathbf{n}_2} + \delta_{j,i-\mathbf{n}_1+\mathbf{n}_2}) b_{2j}^\dagger b_{2j}
\end{aligned} \tag{14}$$

The above expressions are also consistent with the leading contributions from our numerical results shown in Table II and Table III.

We now discuss the effect of sub-leading terms that are not included in Eq. 14. We divide the sub-leading interactions into two parts: density-density and normalized hopping. The density-density part takes the form of $v_{ij,\mu\nu} n_{i\mu} n_{j\nu}$. We found such terms to favor the same order as the leading interactions, This part would only modify the phase boundaries. The normalized hopping term can be written as $V_{ijk,\mu\nu\alpha} n_{i\mu} d_{j\nu}^\dagger d_{k\alpha}$. At the mean-field level, we can decouple this term as $V_{ijk,\mu\nu\alpha} (\langle n_{i\mu} \rangle d_{j\nu}^\dagger d_{k\alpha} + n_{i\mu} \langle d_{j\nu}^\dagger d_{k\alpha} \rangle)$. It would normalize the hopping strength and favors some bond orders. However, the average strength of the normalized hopping term is about 80% smaller than the dominant terms. In summary, the approximate interactions in Eq. 14 already faithfully describe the original kagome system.

D. Entwined order parameters

In this section, we discuss the connections between order parameters in WO basis and kagome basis. The charge and spin order parameters along x direction in the kagome basis can be written as

$$\begin{aligned}
\phi_q^c &= \langle P c_k^\dagger c_{k+q} P \rangle \sim \langle \sum_{\alpha} w_{\alpha\nu k} w_{\alpha\mu k+q}^* b_{k\nu}^\dagger b_{k+q\mu} \rangle \\
\phi_q^x &= \langle P c_k^\dagger \sigma^x c_{k+q} P \rangle \sim \langle \sum_{\alpha} \sigma_{\alpha\gamma}^x w_{\alpha\nu k} w_{\gamma\mu k+q}^* b_{k\nu}^\dagger b_{k+q\mu} \rangle
\end{aligned} \tag{15}$$

Combining the above expressions with Eq. 13, we find the following approximate formula as shown in the main text

$$\begin{aligned}
\phi_q^c &\sim \frac{4 + e^{iq\mathbf{n}_1} + e^{-iq\mathbf{n}_2}}{2} A^2 (n_{1,q} + n_{2,q}) + \frac{2 - e^{iq\mathbf{n}_1} - e^{-iq\mathbf{n}_2}}{2} A^2 (n_{1,q} - n_{2,q}) \\
\phi_q^x &\sim \frac{2 - e^{iq\mathbf{n}_1} - e^{-iq\mathbf{n}_2}}{2} A^2 (n_{1,q} + n_{2,q}) + \frac{4 + e^{iq\mathbf{n}_1} + e^{-iq\mathbf{n}_2}}{2} A^2 (n_{1,q} - n_{2,q})
\end{aligned} \tag{16}$$

This suggests a single charge order (or spin order) in the WO basis produces entwined charge and spin orders in the kagome basis. In Fig. 8, we illustrate this by plotting the real-space pattern of the DW_t phase (charge order in the WO basis).

E. U(1) Slave-spin method

In the $U(1)$ slave spin method, we rewrite the electron operators as $b_{i\mu} = S_{i\mu}^- f_{i\mu}$ where f is the fermion operator and S^- is the spin operator. The original Hilbert space can be mapped onto an extended space of slave spins and f fermions according to the following correspondence:

$$\begin{aligned}
|1\rangle_b &= |1\rangle_f |\uparrow\rangle_s \\
|0\rangle_b &= |0\rangle_f |\downarrow\rangle_s
\end{aligned} \tag{17}$$

To project out the unphysical degree of freedom, we enforce the constraint: $S_{i\mu}^z + \frac{1}{2} = f_{i\mu}^\dagger f_{i\mu}$

The slave spins carry the $U(1)$ charge which allows us to rewrite the interactions as

$$b_{i\mu}^\dagger b_{i\mu} b_{j\mu'} b_{j\mu'} = (S_{i\mu}^z + \frac{1}{2})(S_{j\mu'}^z + \frac{1}{2}) \tag{18}$$

For the non-local interactions with $i \neq j$, we further decouple it via

$$(S_{i\mu}^z + \frac{1}{2})(S_{j\mu'}^z + \frac{1}{2}) \sim -\langle S_{i\mu}^z + \frac{1}{2} \rangle \langle S_{j\mu'}^z + \frac{1}{2} \rangle + \langle S_{i\mu}^z + \frac{1}{2} \rangle (S_{j\mu'}^z + \frac{1}{2}) + (S_{i\mu}^z + \frac{1}{2}) \langle S_{j\mu'}^z + \frac{1}{2} \rangle \tag{19}$$

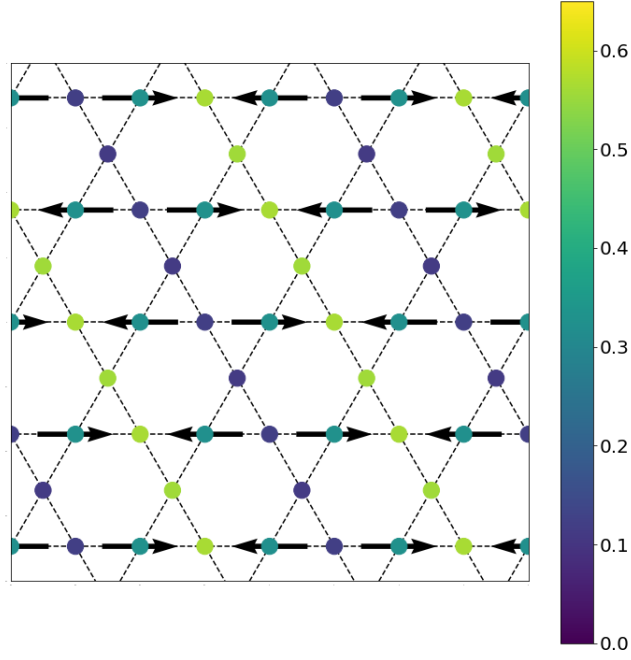


FIG. 8. Real space pattern of the DW_t . The color represents the filling of each site and the arrow denotes the magnitude and direction of in-plane local moment. We can observe a collinear order in the charge channel that is decorated by a collinear order in the spin channel.

Then the effective Hamiltonian is

$$H_f = \sum_{ij} t_{ij}^{\mu\mu'} \eta_{ij} f_{i\mu}^\dagger f_{j\mu'} + \sum_i \lambda_{i\mu} f_{i\mu}^\dagger f_{i\mu} \quad (20)$$

$$H_S = \sum_{ij, \mu\mu'} t_{ij}^{\mu\mu'} (\chi_{ij}^{\mu\mu'} \langle z_{i\mu}^\dagger \rangle z_{j\mu'} + \text{h.c.}) - \sum_{i, \mu} \lambda_{i\mu} S_{i\mu}^z + \sum_i u_{1122} (0, 0, 0) (S_{i,1}^z + \frac{1}{2}) (S_{i,2}^z + \frac{1}{2}) + \sum_{i\mu} m_{i\mu} (S_{i\mu}^z + \frac{1}{2})$$

where λ_μ is the Lagrangian multiplier and operators $z_{i\mu} = \frac{1}{\sqrt{1/2 + S_{i\mu}^z}} S_{i\mu}^- \frac{1}{\sqrt{1/2 - S_{i\mu}^z}}$ are introduced to obtain the correct non-interacting limit. Other parameters are determined self-consistently by

$$\begin{aligned} \eta_{ij}^{\mu\mu'} &= \langle z_{i\mu}^\dagger \rangle_{H_S} \langle z_{j\mu'} \rangle_{H_S} \\ \chi_{ij}^{\mu\mu'} &= \langle f_{i\mu}^\dagger f_{j\mu'} \rangle_{H_f} \\ m_{i\mu} &= \sum_{j, \nu} u_{\mu\mu\nu\nu} (0, j, j) \langle S_{i+j\nu}^z + \frac{1}{2} \rangle_{H_S} \end{aligned} \quad (21)$$

Effectively, our slave-spin method introduces a wave-function Ansatz: $P_G |HF\rangle$ and variationally find the state with the lowest energy. P_G is a Gutwiler projector that disfavors double occupancy and $|HF\rangle$ denotes the ground state of a free electrons model with Hartree-Fock contributions.

At each (U, V') , we randomly initialized 15 sets of variables $(\eta_{ij}^{\mu\mu'}, \chi_{ij}^{\mu\mu'}, m_{i\mu}, \lambda_{i\mu})$ and find self-consistent solutions of each initialization. Any type of three-sublattice and two-sublattice orders are allowed in the calculations, and other types of orders are not favored by interactions. The final ground state corresponds to the solution with the lowest free energy. In addition, we set the temperature to be $\beta W = 1000$.